PAPER

Pulsed operation of a ring Stark decelerator

IOP Publishing Journal of Physics B: Atomic, Molecular and Optical Physics
J. Phys. B: At. Mol. Opt. Phys. **51** (2018) 165101 (10pp) https://doi.org/10.1088/1361-6455/aad1b0

Pulsed operation of a ring Stark decelerator

Yomay Shyur, Jason A Bossert and H J Lewandowski

JILA, NIST, and Department of Physics, University of Colorado, Boulder, Colorado 80309-0440, United States of America

E-mail: yomay.shyur@colorado.edu

Received 10 May 2018, revised 22 June 2018
Accepted for publication 6 July 2018
Published 24 July 2018

Abstract

Stark deceleration is a technique that uses time-varying inhomogeneous electric fields to decelerate polar molecules for various molecular beam and trapping experiments. New ring-geometry Stark decelerators with continuously varying voltages offer a method to produce a more intense source of molecules than in the more typically used crossed-pin geometry Stark decelerators. However, this new technique, traveling-wave Stark deceleration, is more experimentally challenging due to the electronic requirements. A third method, pulsed-ring Stark deceleration, uses ring-geometry electrodes with high-voltage pulses to decelerate molecules. The discrete voltages make it easier to implement, and it is more efficient in certain situations due to an increased longitudinal potential gradient. Here, we present an experimental realization of a ring-geometry Stark decelerator using both continuously varying and discrete voltages. Using the pulsed-ring method, we demonstrate a newly accessible low-velocity regime for moderate peak voltages on ring electrodes. This opens up the opportunity to efficiently decelerate various molecular species using a medium length decelerator. A comparison of experimental and simulated results between traveling-wave and pulsed-ring Stark deceleration is presented along with a simple model for determining when each mode is more efficient.

Keywords: Stark deceleration, molecular beams, cold molecules

(Some figures may appear in colour only in the online journal)

1. Introduction

Stark deceleration uses spatially inhomogeneous and time-varying electric fields to decelerate neutral polar molecules, and produces a beam of slow molecules with a tunable average final velocity. These beams can be used for high-resolution spectroscopy [1], collision physics [2], measuring radiative lifetimes of molecules [3, 4], and tests of fundamental physics [5–7]. The molecules from a Stark decelerator can also be loaded into electrostatic [8–10], magnetic [11, 12], and ac traps [13–15], or used in crossed beam [16–19], beam-trap [20, 21], and co-trapped experiments [22]. Such experiments are often limited by the number of successfully decelerated molecules. Improvements to the decelerator efficiency, the percentage of molecules in the initial pulse that are successfully decelerated, would benefit these types of studies.

The first Stark decelerator, referred to in this paper as the pulsed-pin Stark decelerator (PPSD), was constructed in 1999 by Bethlem *et al* [23]. It used high-voltage switches to alternate between two static voltage configurations on pairs of crossed-pin electrodes. Switching between these voltage configurations produces a discretely moving Stark potential well to decelerate molecules. Molecules only within a range of positions and velocities will be decelerated. This portion of phase space is called the phase-space acceptance. Ideally, it would be well filled with molecules. PPSD has well-characterized instabilities and loss mechanisms that are enhanced at low final velocities [24]. Particularly, coupling between the longitudinal and transverse motion and over focusing leads to unstable regions within the phase-space acceptance. The decrease in phase-space acceptance drastically reduces efficiency when decelerating to low velocities required for trapping, or when spending long times at velocities $<100\,\mathrm{m\ s^{-1}}$ in the decelerator. Although different timing schemes and operating modes can improve the performance of the traditional Stark decelerator [25–27], the crossed-pin electrode geometry fundamentally limits efficiency due to longitudinal and transverse coupling.

The loss present in pin decelerators can be mitigated using ring-shaped electrodes and a fundamentally different mode of applying voltages to the electrodes: chirped

sinusoidally varying voltages. This produces a traveling-wave potential well that continuously guides or decelerates the molecular beam, as opposed the pulsed nature of PPSD. Traveling-wave Stark deceleration (TWSD) has two characteristic differences compared to PPSD: the cylindrically symmetric electrode geometry and continuously, as opposed to discretely, varying voltages, which produce a genuine moving potential well. This leads to an inherently stable deceleration process that has a true three-dimensional (3D) trapping potential and a well-filled phase-space acceptance. These factors allow for more efficient deceleration due to the continuous and cylindrically symmetric nature of this deceleration mode. Meek *et al* [28] first demonstrated the idea for spatially modulated potential wells on a microstructured chip used to guide and then decelerate metastable CO molecules [29, 30]. The first use of macroscopic traveling-wave Stark potentials with a ring-geometry decelerator was experimentally shown in 2010 by Osterwalder *et al* [31] using a beam of CO, which was decelerated from 288 m s^{-1} to 144 m s^{-1}.

While TWSD has many advantages, it is more challenging to implement than PPSD because it requires high-voltage analog amplifiers with demanding specifications to generate the moving Stark potential wells. The sinusoidal voltage must have an initial frequency such that the Stark potential well containing the molecules moves with the same initial velocity as the molecular beam. The frequency of the sinusoidal voltages must then be smoothly chirped down to a frequency such that the velocity of the Stark potential well formed by the voltages matches the desired final beam velocity. Thus, the amplifiers require a large bandwidth to decelerate a typical molecular beam to rest. The chirp rate of the sinusoidal voltage will be determined by the initial and final velocities and the length of the decelerator. For a fixed ring geometry, the magnitude of the maximum allowable deceleration is set by the bandwidth of the high-voltage amplifiers, maximum output voltage of the high-voltage amplifiers, and length of the decelerator.

Early TWSD experiments were limited by the lack of availability of high-voltage amplifiers with a large bandwidth. The amplifiers used to generate the voltages for the electrodes in the first TWSD experiment operated at ±8–10 kV with 10–30 kHz sinusoidal voltages [31, 32]. The limited bandwidth of the amplifiers meant that the decelerator could achieve only moderate deceleration and the molecules could not be brought to rest. Commercial amplifiers (Trek 5/80), which are capable of a larger frequency range (0–60 kHz) and outputs up to ±5 kV, make it possible to decelerate a supersonic beam down to rest with a decelerator that is several meters long. For example, a beam of SrF seeded in Xe with an initial velocity of 290 m s^{-1} would require a ∼5 m long decelerator [33]. Amplifiers with slightly limited maximum voltages such as these are particularly useful for TWSD of heavy molecules used in precision measurements, since the electric fields produced are low enough to keep the molecules in the weak-field seeking regime, where the Stark energy increases with increasing electric field [34]. To date, YbF [35] and SrF [33] have been decelerated using TWSD and the longest demonstrated decelerator (4 m) slowed SrF from 290 to 120 m s^{-1} using ±5 kV amplifiers [36].

To overcome the limitations of PPSD and the demanding amplifier specification of TWSD, a combination of both Stark deceleration methods can be used. In this combination technique, a pulsed-pin Stark decelerator decelerates molecules to longitudinal velocities around 100 m s^{-1}, and then a traveling-wave Stark decelerator decelerates the molecules to rest [37]. This scheme is able to take advantage of the cylindrical symmetry of the ring geometry at low velocities to avoid the low-velocity losses of the pulsed-pin Stark decelerator, but it relaxes the requirement to have either extremely high maximum voltages or a very long decelerator to reach electrostatically trappable conditions. Using this combination technique, NH_3/ND_3 and CH_3F have been trapped, manipulated, and adiabatically cooled within the ring decelerator [37–40].

Complete TWSD of a supersonic beam moving at 300–450 m s^{-1} to rest has been challenging to achieve due to electronic and hardware requirements. Based on simulations, an alternative running mode for operating a ring-geometry decelerator has been proposed by Hou *et al* [41], and uses pulsed voltages on ring electrodes. The duration of the pulses is varied in an identical manner to that of PPSD. This pulsed-ring Stark deceleration (PRSD) method takes advantage of the cylindrical symmetry provided by the rings and is simpler to implement than TWSD since it uses commercial high-voltage switches instead of high-voltage analog amplifiers. In this paper, we present experimental results of this new PRSD scheme in comparison with TWSD and simulations. We find that for certain voltage configurations PRSD produces comparable results to TWSD, similar to the results of Hou *et al.* However, some peak voltage and accelerations yield conditions where it is advantageous to run PRSD over TWSD. We discuss a simple method for determining which mode is preferable based on the desired final molecule packet properties.

2. Experiment

The experimental setup for demonstrating both deceleration modes is shown in figure 1. Both experiments begin with a piezoelectric-actuated pulsed valve that creates a pulsed supersonic beam of 2% fully deuterated ammonia (ND_3) in krypton. A skimmer ∼20 cm downstream of the valve collimates the molecular beam and allows for differential pumping between the source and decelerator chambers. The decelerator begins 3 mm behind the skimmer, and consists of 624 rings mounted in eight longitudinal stainless steel rods such that every eighth ring is electrically connected (similar to [31]). Each ring is made of 1.02 mm diameter tantalum wire, and has a 4 mm inner diameter and center-to-center spacing of l, which for the decelerator discussed here is $l = 2.03$ mm. The full decelerator is just over 1.25 meters long. For the work presented here, ND_3 molecules are decelerated from 415 m s^{-1} down to final velocities of 220 m s^{-1} for TWSD and 150 m s^{-1} for PRSD. ND_3 molecules at the end of the decelerator are ionized in a 2 + 1 REMPI scheme using 317 nm photons [42]. Two stainless steel plates, which are electrically isolated from

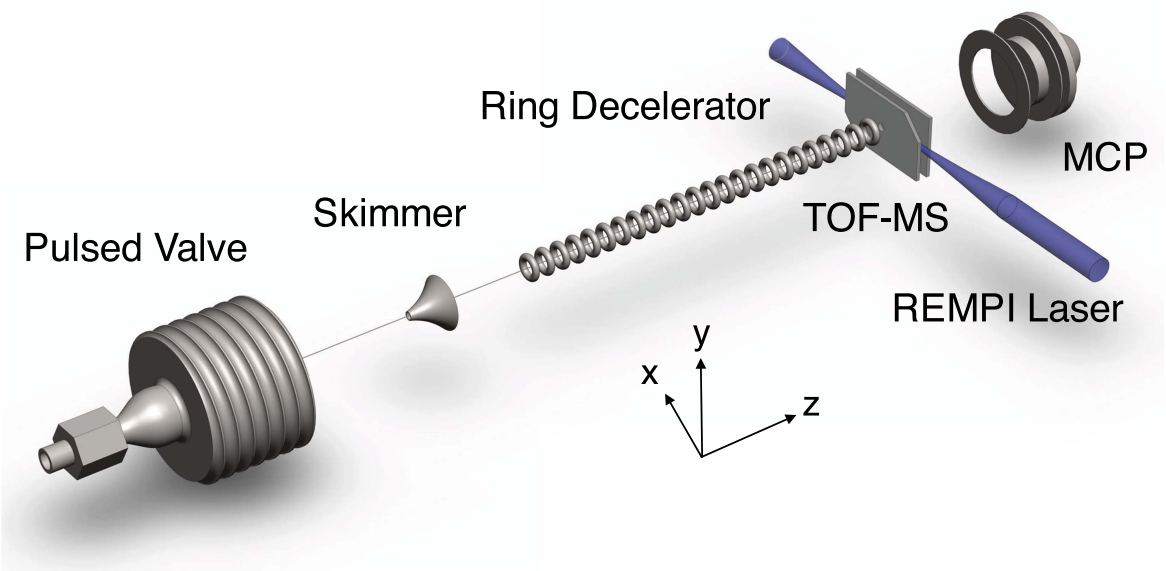

Figure 1. A schematic of the experimental setup which includes, from left to right, a pulsed valve, skimmer, ring decelerator, time-of-flight mass spectrometer (TOF-MS), detection laser, and microchannel plate detector (MCP). Not all decelerator rings are depicted. The full decelerator contains 624 rings. The longitudinal stainless steel mounting rods are also not shown. The entire system is contained inside a differentially pumped vacuum chamber.

the decelerator, are mounted after the rings. They form the time-of-flight mass spectrometer and accelerate ionized molecules into the microchannel plate detector, where the measured current is proportional to the number of ionized molecules.

The voltage sequences for the two deceleration modes create longitudinal potential wells with different ring periodicities and gradients. In the work presented here, both modes of deceleration use maximum voltages of ± 7 kV on the electrodes. This decelerator was designed for ± 10 kV TWSD, which has a maximum voltage difference between rings of 7.7 kV. Since the decelerator was not voltage conditioned for higher electrode-to-electrode voltage differences, PRSD is limited ± 7 kV for this particular configuration. PRSD uses four commercial high-voltage switches and TWSD uses eight custom home-made high-voltage amplifiers. With electronics for both techniques prepared, the switch from PRSD to TWSD takes less than a day of work. Figure 2 shows a longitudinal cross section of the ring decelerator in the upper panel and the longitudinal Stark potential for ND_3 for each deceleration mode in the lower panel. The rings are labeled with their rod number, n, from zero through seven. The instantaneous voltages that create the given longitudinal Stark potentials are listed in the table at the top. The left most and right most rings, $n = 4$, are electrically connected, and the voltage and Stark potential pattern is repeated down the length of the decelerator.

The pulsed mode naturally creates wells with greater gradients, which allows it to be more efficient in certain circumstances. While a pulsed-ring configuration with the same well periodicity and gradients as TWSD could be configured, it would be less efficient than the pulsed version presented here. Such a configuration would use the same instantaneous voltages as listed for V_{TWSD} in figure 2 and create the same

Ring (n)	4	5	6	7	0	1	2	3	4
V_{PRSD} (kV)	0	7	0	-7	0	7	0	-7	0
V_{TWSD} (kV)	0	-4.9	-7	-4.9	0	4.9	7	4.9	0

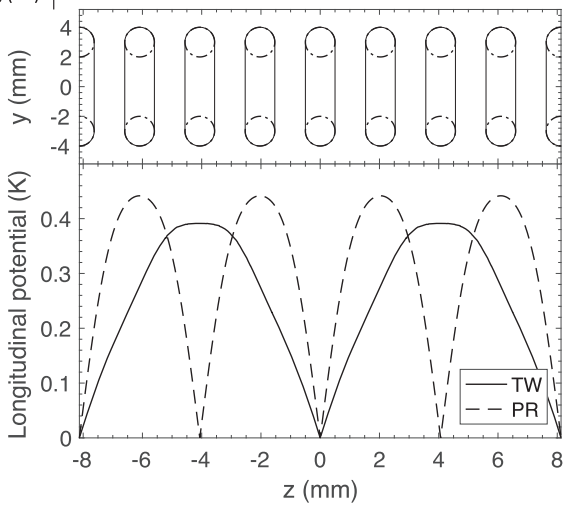

Figure 2. Ring number, applied voltages, positions of electrodes, and longitudinal Stark potentials of ND_3 in units of Kelvin. The table and top panel show the ring number n and instantaneous voltages for both deceleration modes plotted below and the longitudinal cross section of the decelerator rings. The bottom panel shows the TWSD and PRSD Stark potentials along the center axis of the ring decelerator. Both Stark potentials are shown at a time when the bottom of the potential well is centered at a ring.

instantaneous potentials. The bottom of the Stark potential well would shift by two rings each time and there would only be half the number of switching stages. This reduction in deceleration stages, along with the reduced gradient, greatly diminishes the decelerating capabilities of such a configuration and thus it is not used here.

2.1. Deceleration modes

For the PRSD configuration, each rod is connected to one of four Behlke HTS 201-03-GSM-HFB high-voltage switches. These switches are used to produce two voltage configurations that alternate in time. The two voltage configurations produce two Stark potential well configurations, one of which is depicted in the bottom panel of figure 2. A detailed description of the electrode and voltage configuration can be found in [41]. The time interval between switching from one configuration to another is dictated by the velocity of the molecular beam. These voltages produce an on-axis longitudinal Stark potential with the bottom of the well shifted by l between the two configurations, similar to the pin decelerator. The timing sequence for switching the voltages on the electrodes is calculated in a similar fashion, using phase angles, as that of a pulsed-pin Stark decelerator [43].

For the TWSD configuration, eight analog high-voltage amplifiers are used, one for each rod. These supply the rings with chirped sine wave voltages, which have a fixed phase offset relative to one another. The amplifiers (gain = 12,000) are driven by an arbitrary waveform generator (GaGe CompuGen 8152). The high-voltage linear amplifiers used in this work were designed and constructed in-house. They were tested up to ±10 kV and in the frequency range of 1–30 kHz on the bench, but were operated at ±7 kV and in the frequency range of 13–25.5 kHz for this work. These specifications correspond to a molecular beam with velocities from 415 m s^{-1} down to 210 m s^{-1}. While the amplifiers have a bandwidth of 30 kHz down to DC, the full bandwidth was not utilized since the lower maximum voltage on the rings results in a shallower molecule trap. The set length of our decelerator and this shallower trap did not allow for deceleration down to rest for this particular experiment. However, with ±10 kV outputs from the amplifiers, the ND_3 molecules with an initial velocity of 415 m s^{-1} could be brought to rest.

Each amplifier applies the chirped sine wave voltage V_n, for a given rod n, of

$$V_n(t) = V_a \sin\left(\frac{2\pi n}{8} - \frac{2\pi}{8l}\left(v_i t - \frac{1}{2}at^2\right)\right), \quad (1)$$

where V_a is the maximum output voltage, v_i is the initial velocity of the molecular beam, a is the acceleration applied by the decelerator, and the $\frac{2\pi n}{8}$ term is the phase shift between rods. The acceleration is given by

$$a = \frac{v_f^2 - v_i^2}{2L}, \quad (2)$$

where v_f is the final velocity of the molecular beam and L is the overall length of the decelerator. It is important to note that one period of the sine wave extends over eight ring electrodes and corresponds to two Stark potential wells (see figure 2). This results from the Stark potential energy depending on the magnitude of the electric field and not the direction.

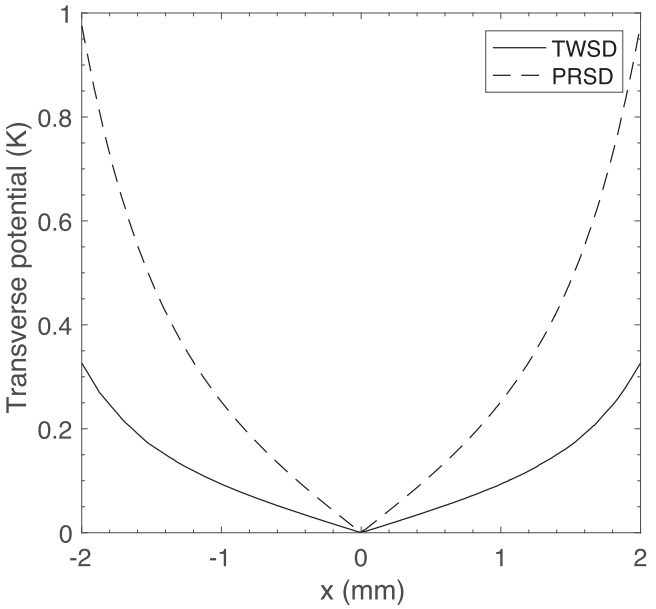

Figure 3. The instantaneous TWSD and PRSD transverse Stark potentials in the x direction for the voltage configuration in figure 2 and at z = 0 mm.

3. Simple model of deceleration

The Stark potential wells for each deceleration method give a basic picture into which molecules within the initial phase space can be decelerated. Figure 3 shows the transverse potentials for both TWSD and PRSD for the voltage configuration in figure 2 taken at z = 0 mm, the bottom of the longitudinal well for both modes. The transverse potential is identical in the x and y directions due to the cylindrical symmetry of the decelerator. The lower panels of figures 2 and 3 show that for the same peak voltage PRSD has a larger potential well gradient in both the longitudinal and transverse directions due to the reduced ring periodicity of the configuration.

The larger potential well gradient is particularly important in the longitudinal direction. To predict which molecules will be successfully decelerated (i.e. within the phase-space acceptance), we consider the effects of the acceleration on the Stark potential well. Deceleration of the Stark potential well is the equivalent of adding a fictitious potential $U_f = maz$ to the longitudinal Stark potential in figure 2, where m is the mass of the molecule and z is the longitudinal distance from the center of the Stark potential well. For both modes, the average acceleration is determined only by decelerator length, v_i, and v_f. The acceleration is applied constantly in TWSD, but is time-averaged in PRSD, where instantaneous accelerations are higher. Figure 4 shows the central TWSD and PRSD Stark potential wells from figure 2 with an acceleration of 0 km s^{-2}, −32.5 km s^{-2}, and −47.1 km s^{-2} added to the Stark potential. For a beam with v_i = 415 m s^{-1}, this corresponds to v_f = 415 m s^{-1}, v_f = 300 m s^{-1} and v_f = 230 m s^{-1} respectively. This additional fictitious potential lowers the downstream potential well wall since a is negative, and the effect is referred to as the potential well tilt. (The tilt model of a Stark

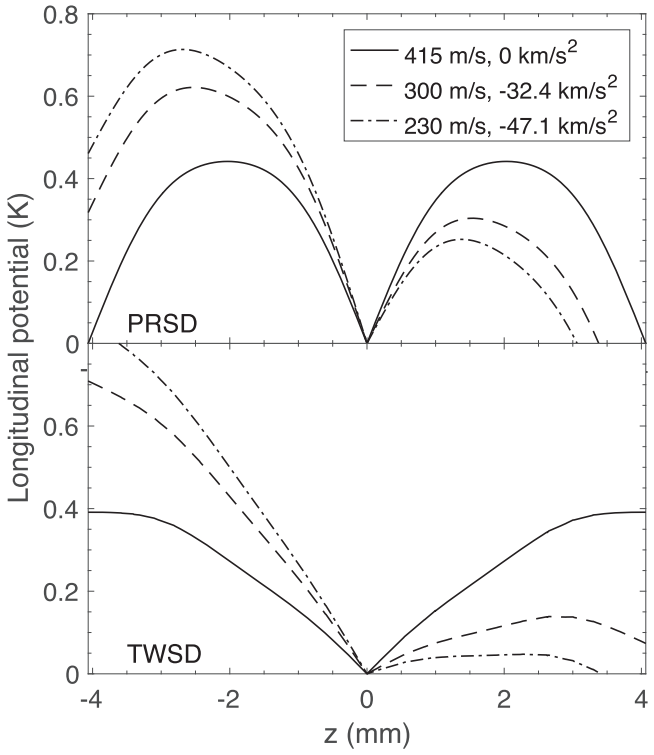

Figure 4. The PRSD (top) and TWSD (bottom) Stark potential wells with applied linear fictitious potentials for $a = 0\,\mathrm{km\,s^{-2}}$ (solid), $a = -32.5\,\mathrm{km\,s^{-2}}$ (dashed), and $a = -47.1\,\mathrm{km\,s^{-2}}$ (dot dashed). For a beam with $v_i = 415\,\mathrm{m\,s^{-1}}$, this corresponds to $v_f = 300\,\mathrm{m\,s^{-1}}$ and $v_f = 230\,\mathrm{m\,s^{-1}}$ respectively.

decelerator is discussed more in depth in [44].) As a increases, the well tips over more and cannot contain and decelerate as many molecules. An acceleration of $-47.1\,\mathrm{km\,s^{-2}}$ shows how the TWSD Stark potential well is aggressively tilted to the point of almost having no trap depth. Too much acceleration, and thus too much tilt, leads to a small phase-space acceptance and deceleration efficiency.

For either mode, too large an acceleration means no molecules are phase stable inside the Stark potential well. The maximum acceleration where the phase-space acceptance is finite is set by the gradient and height of the Stark potential well. A larger Stark potential gradient allows for more acceleration before the well can no longer hold molecules. In figure 4 for $a = -47.1\,\mathrm{km\,s^{-2}}$, PRSD still has significant well depth, while TWSD has almost none. This is because PRSD has a larger Stark potential gradient. The Stark potential well gradient is set by the deceleration mode and physical decelerator geometry. Decelerating to low final velocities requires either a low initial velocity, which is set by the gas used in the supersonic expansion, or a long decelerator. For the same V_a on the electrodes, the pulsed configuration produces a Stark potential well with a larger gradient in both the longitudinal and transverse directions and a smaller volume because the well only spans $2l$ while the traveling-wave well spans $4l$. This allows the PRSD well to tilt more and be stable at larger accelerations than the TWSD well even though it has a smaller volume.

4. Simulations

In addition to the experimental results, we use Monte Carlo simulations to help interpret and illustrate the differences between the two operating modes. These semi-classical molecular trajectory simulations allow us to explore a wide parameter space that is not yet accessible in the current experimental setup. The simulation starts by creating a packet of molecules at the location of the pulsed valve. The molecules have a Gaussian distribution of initial positions and velocities. The molecular packet is allowed to propagate through a region with no electric field to the entrance of the decelerator. Once the molecules enter the decelerator, their trajectories are determined using a 3D matrix of accelerations derived from Stark potentials modeled by the commercial finite element solver COMSOL. Once the packet of molecules reaches the end of the decelerator both the phase-space distribution (observation at a set time) and the time-of-flight information (observation at a set z-position) are recorded.

Typical initial packets contain between 1 and 8 million molecules that are sampled from a distribution that has full-width half maximum of $\Delta x = \Delta y = 3\,\mathrm{mm}$, $\Delta z = 30\,\mathrm{mm}$, $\Delta V_x = \Delta V_y = 5\,\mathrm{m\ s^{-1}}$, and $\Delta V_z = 30\,\mathrm{m\ s^{-1}}$. This packet extends beyond the phase-space acceptance of the decelerator.

Since the Stark potential well shapes for both deceleration modes are spatially periodic, the electric field models for determining the molecule accelerations inside the decelerator do not have to span the entire length of the decelerator. Instead, a modular approach can be taken. The position dependent molecular accelerations are calculated from electric field models for a unit cell of three (nine) rings for PRSD (TWSD). Then, a shift of the longitudinal coordinates within the unit cell allows for molecules to propagate along the decelerator without a model of the entire decelerator. The number of position dependent 3D acceleration models required depends on the operating mode. For PRSD, there are only two voltage configurations and the shape of the Stark potential well is the same for both configurations, but shifted by l. Therefore, only one acceleration model is required and is longitudinally shifted by l each time the high voltage is switched. For TWSD, there is a continuum of voltage configurations corresponding to the sinusoidally varying voltages on the rods. This is modeled using 25 time steps between the peak of the sine wave being on rod n to the peak being on the subsequent rod $n + 1$. Once the simulations have cycled through all 25 modeled time steps the entire model is longitudinally shifted by l.

5. Experimental results and analysis

5.1. Deceleration at 7 kV

We performed experimental measurements for both PRSD and TWSD at $\pm 7\,\mathrm{kV}$ using the setup described in section 2 and compared them to simulations. All experiments use a molecular beam with an initial velocity of $415\,\mathrm{m\ s^{-1}}$. The beam was decelerated to various final velocities. Figures 5, 6

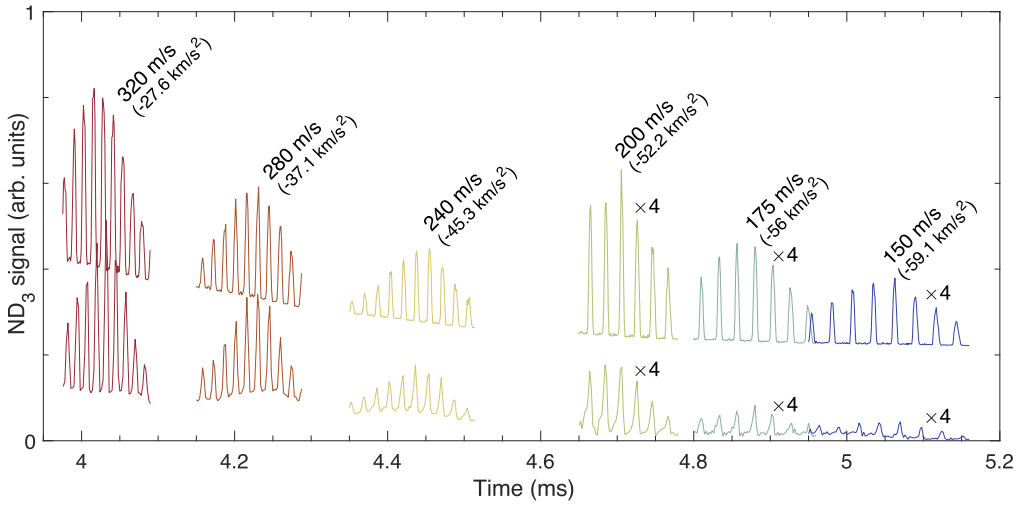

Figure 5. Time-of-flight traces of a molecular beam decelerated with PRSD from an initial velocity of 415 m s^{-1} down to the labeled final velocities using the indicated accelerations. The three slowest packet signals have been multiplied by a factor of 4. The top row shows the results of the simulations and the bottom row shows the experimental measurements. The experimental results consist of data points 2 μs apart and represent the average of 192 individual measurements. The error bars on the experimental data are a similar magnitude to the width of the plotted line. The results of the simulations have been vertically offset for clarity.

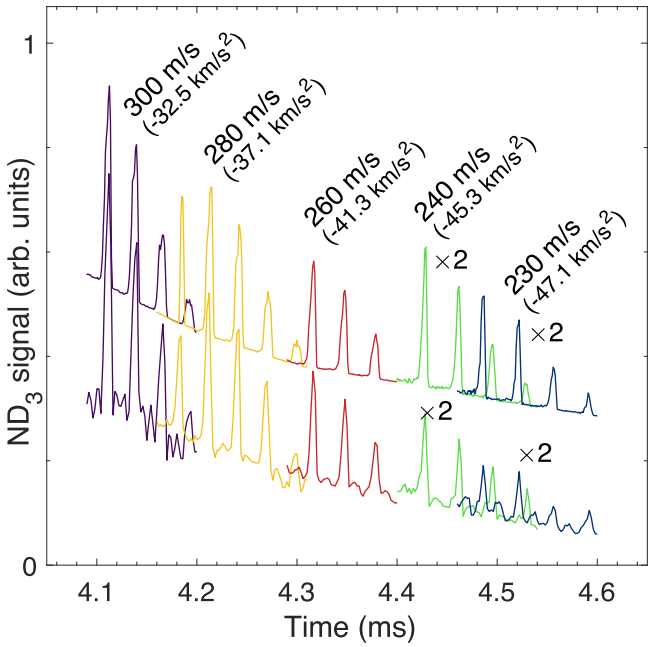

Figure 6. Time-of-flight traces of a molecular beam decelerated with TWSD from an initial velocity of 415 m s^{-1} down to the labeled final velocities using the indicated accelerations. The two slowest packet signals have been multiplied by a factor of 2. The top row shows the results of simulations and the bottom row shows the experimental measurements. The experimental results consist of data points 2 μs apart and represent the average of 192 individual measurements. The error bars on the experimental data are a similar magnitude to the width of the plotted line. The results of the simulations have been vertically offset for clarity.

shows PRSD (TWSD) signals for decelerated ND_3 packets as a function of arrival time for selected final velocities. Both figures have results from the simulated decelerated packets on the top and the experimental data on the bottom. There are more decelerated peaks in each packet than shown, but, for clarity, only the central and a couple adjoining peaks are displayed. Both figures have the same vertical scale. The arrival time between peaks in PRSD is more closely spaced than in TWSD due to the well spanning only $2l$ instead of $4l$. Since there is not enough deceleration to separate the decelerated packets completely from the initial pulse, the baselines of the signals are not zero and sit on top of the low-velocity tail of the initial molecular beam.

With the same initial velocity, $v_i = 415$ m s^{-1}, and large accelerations such that $v_f < 220$ m s^{-1}, TWSD no longer results in observable decelerated signal, but PRSD still produces clear peaks. PRSD produces observable decelerated molecules down to $v_f = 150$ m s^{-1}. While TWSD produces more decelerated ND_3 than PRSD at $v_f > 230$ m s^{-1}, it does not produce clearly decelerated packets over the same large velocity range as PRSD, and the amplitude of decelerated peaks decreases more rapidly than in PRSD as the acceleration increases.

The simulations accurately predict the shape and arrival times of the molecules. While the amplitude of the experimental results and simulation are comparable at higher final velocities (small acceleration), the experimental signal is lower than the signal expected from the simulation at lower final velocity (large acceleration). These deviations at large accelerations are likely due to imperfections in electrode rings and voltages. This may arise from individual ring misalignment or, for TWSD, deviations in amplifier output voltage from an ideal sine wave. While careful frequency tuning and calibration can mitigate amplifier fluctuations, any imperfections add jitter to the Stark potential well. At large accelerations, jitter may distort the already shallow Stark potential well to the point that many normally phase-stable molecules fall out. However, this would be less of a concern for a deeper potential well with less tilt such that imperfections in the well are small compared to the downstream Stark potential well height of the tilted well.

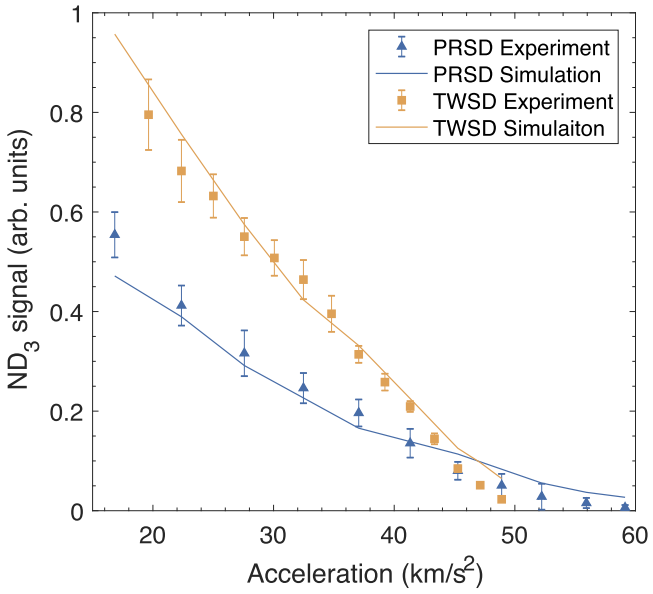

Figure 7. ND_3 signal verses acceleration for both TWSD (yellow squares) and PRSD (blue triangles). The experimental measurements are given by individual points and the results from Monte Carlo simulations by a line. The error bars on the experimental data points are dominated by the choice of integration baseline. The cross-over from TWSD to PRSD producing more decelerated molecule signal occurs near 46 km s^{-2}.

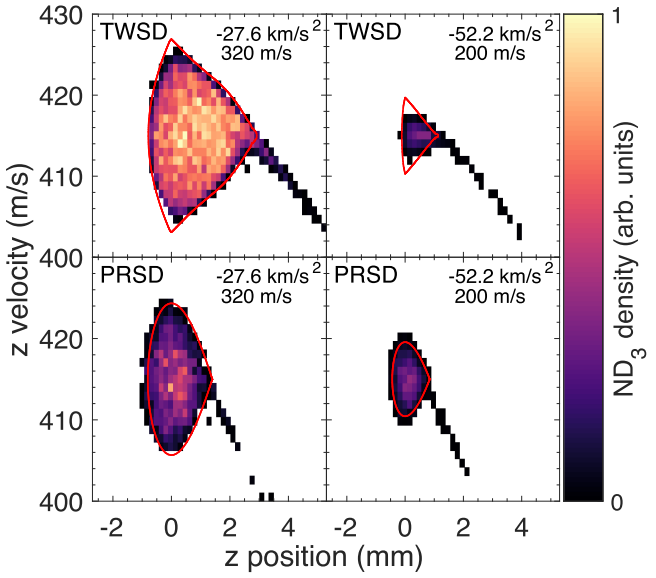

Figure 8. Longitudinal phase-space plots with TWSD in the top row and PRSD in the bottom row. The graphs in left column are given for an acceleration of -27.6 km s^{-2} and the graphs in the right column are given for an acceleration of -52.2 km s^{-2}. For an initial velocity of 415 m s^{-1}, this would be a final velocity of 320 m s^{-1} and 200 m s^{-1} respectively. The solid-red lines are the 1-dimensional separatricies. There is no significant structure in the phase-space acceptance in either deceleration mode.

We use the integrated signal above the baseline in the central peak of each packet to determine and quantify the trade-off between the two modes. The integrated signal for both experimental and simulated results is shown in figure 7. The x-axis has been changed from final velocity to acceleration using equation (2), so that the results can be applied to different initial velocities. Now, the trade-off between the two modes is clear. There is a cross-over point between the decelerated signals in TWSD and PRSD. For low accelerations TWSD yields higher overall signal, but at accelerations greater than -46 km s^{-2} PRSD yields higher signal. Additionally, PRSD has detectable decelerated packets at accelerations above -50 km s^{-2} while TWSD does not. Therefore, if the desired result is a very low-velocity molecular beam, PRSD is preferable for this given electrode voltage and configuration.

5.2. Phase-space acceptance

Another method of examining the cross-over point between the two deceleration modes is to examine the phase-space acceptance, the range of initial molecule positions and velocities that will be decelerated. We define a cross-over point as the acceleration value where at higher accelerations PRSD begins to produce more decelerated signal than TWSD. One-dimensional (1D) longitudinal (z-axis) phase-space boundary calculations, done in the same manner as [43], are useful for determining the separatrix, which is the boundary between stable and unstable molecular orbits in phase space. Figure 8 shows two-dimensional phase-space histograms of all molecules in the central decelerated peak and longitudinal phase-space separatricies for PRSD and TWSD above and below the cross-over point. The phase-space distribution has $z = 0$ as the entrance of the decelerator. Only molecules from the initial distribution that are successfully decelerated and in the central peak are plotted; all other molecules are not shown.

Both modes of deceleration have well-filled phase spaces in both the longitudinal and transverse directions, which differs from the structured phase spaces that are seen in PPSD [24, 26]. Thus, the trade-off in total decelerated signal comes from the change in phase-space area and not phase-space filling. From a final velocity of 320 m s^{-1} to 200 m s^{-1} the phase-space acceptance area of TWSD decreases significantly more than in PRSD. This is due to the significant decrease in Stark potential well depth from tipping due to the acceleration. While the longitudinal phase-space acceptance captures the phase-space boundary of the decelerated molecules, the area of the phase space does not accurately model the efficiency of the deceleration at different final velocities. Even a 3D phase-space volume calculation fails to model the rate of decrease in experimental signal with increased acceleration. This is because the total number of successfully decelerated molecules is determined by the overlap of the phase-space acceptance with the initial distribution of molecules. To account for the initial distribution of the beam, the deceleration efficiency should be computed using Monte Carlo simulations.

5.3. Determining the optimal deceleration mode

There are many things to consider when determining which type of decelerator to build and which mode to operate in for a particular experiment, including complexity of the apparatus

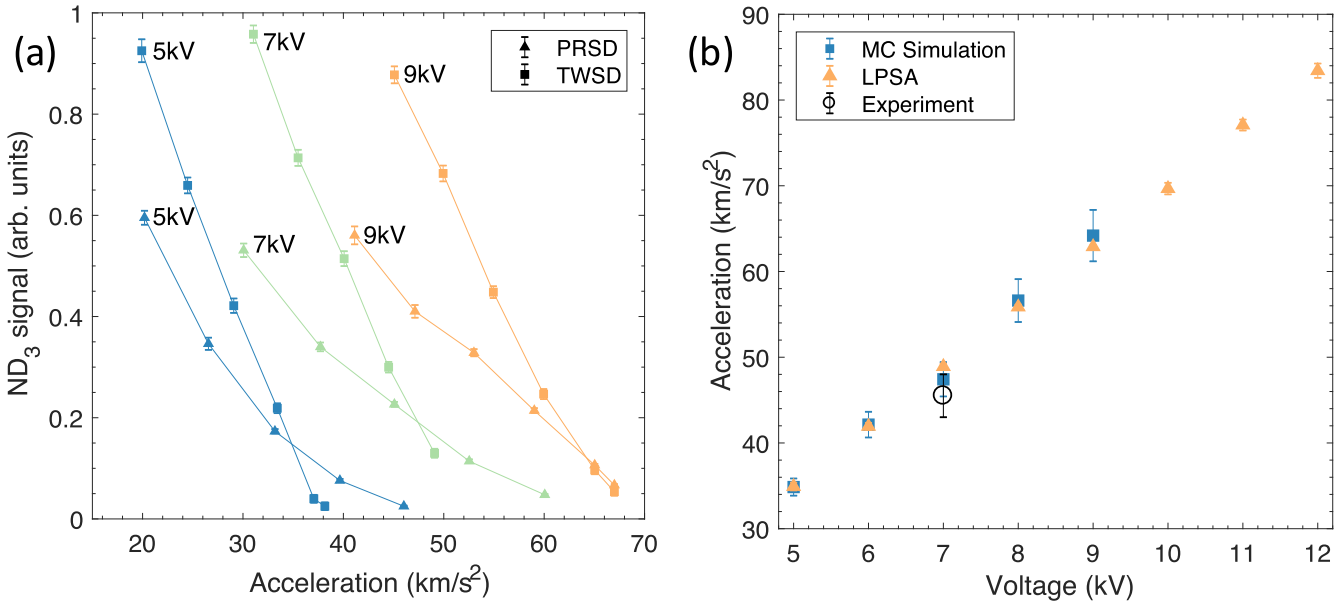

Figure 9. Determination of the efficiency crossing points between TWSD and PRSD. (a) Simulated integrated ND_3 signal verses acceleration for both TWSD (squares) and PRSD (triangles) with peak voltages of 5, 7, and 9 kV. A crossing point exists for all voltages shown. The error on the simulated data is the counting error. (b) The acceleration at the crossing point, where TWSD and PRSD produce similar decelerated molecule signal, calculated using Monte Carlo simulations and 1D longitudinal phase-space acceptance. The error is dominated by the relative slopes of the crossing lines. The crossing point determined by either method is linear with respect to applied voltage. The experimental crossing point (open circle) agrees well with the calculations and simulations. For accelerations greater than the crossing point, PRSD is more efficient at decelerating molecules than TWSD.

and electronics, space, and cost. The trade-off between the two deceleration modes is especially relevant given experimental limitations of a decelerator. To determine which mode is best to use, different voltage regimes were explored using simulations. The same decelerator geometry as previously described was used while changing the peak voltage in both modes. Results of these studies are shown in figure 9(a) for 5, 7, and 9 kV. A crossing point where TWSD and PRSD produce the same signal exists for these voltages and occurs at a larger acceleration for greater electrode voltages.

Generally, TWSD is more efficient for mild accelerations, but for large accelerations, especially at low peak voltages, PRSD may be more efficient. The crossing point may or may not be relevant depending on the parameters of the initial beam and maximum voltage on the electrodes. For example, while a crossing point for 10 kV (not plotted in figure 9(a)) exists, it is not accessible in our decelerator using a molecular beam seeded in krypton. The acceleration to bring ND_3 seeded in krypton from 415 m s^{-1} down to rest is -67.9 km s^{-2} and the crossing point at 10 kV is near -74.3 km s^{-2}. Thus, for 10 kV on the electrodes, a beam seeded in krypton, and this decelerator geometry, TWSD will always produce more ND_3 at all final velocities.

However, at lower peak voltages, PRSD is an important operating mode to consider since it allows access to higher accelerations than TWSD due to the greater Stark potential well gradient. As controlling high-voltages is one of the largest experimental challenges for any Stark deceleration experiment, PRSD may be an important tool to investigate low final molecular velocities given tight voltage constraints. PRSD is easier to implement than TWSD, and allows the beam to reach a lower final velocity, possibly one that can be trappable, without having to build a very long decelerator or obtain analog high-voltage amplifiers.

For a given decelerator length, a quick method of determining which mode will yield more decelerated molecule signal is desirable. Previously, the crossing points between the two modes were determined by integrating time-of-flight traces from Monte Carlo simulations, which is computationally intensive. Instead, the crossing point can be determined using an efficient 1D separatrix calculation.

The 1D separatrix area does not accurately model the decrease in experimental signal with increasing acceleration for either model since it does not account for the initial molecule position and velocity spread. For the separatrix area to accurately predict the rate of decrease of the decelerated peaks the overlap of the initial distribution and the phase space must be known. However, this overlap function affects the phase space of both modes similarly. It does not change the point where their phase-space areas are equal, and can give a good estimate for where the crossing point will occur.

Figure 9(b) shows that the crossing points determined by both Monte Carlo simulations and 1D separatrix calculations are linear with respect to applied acceleration. The experimentally determined crossing point, using the data from figure 7, is plotted with an open circle and agrees with both calculations. The 1D separatrix calculations agree with the Monte Carlo simulations. This is a simple method for determining the crossing point, even if it does not quantify how much better one mode is compared to the other. This simple 1D separatrix calculation easily predicts when one deceleration mode is more efficient than another without having to run Monte Carlo simulations.

6. Conclusion

Stark deceleration has proved to be a reliable source of cold molecules for various applications. However, traditional crossed-pin geometry Stark decelerators have well documented instabilities that reduce their efficiency. An alternative deceleration technology, traveling-wave Stark deceleration, is predicted to nearly eliminate the problems that reduce the number of decelerated molecules. However, the difficulty in creating the required sinusoidally varying high-voltage waveforms for TWSD has limited their integration into experiments. To possibly make the implementation of a ring-geometry decelerator less challenging, we investigated running this type of decelerator in a pulsed mode.

We demonstrated, using experiential measurements and molecular trajectory simulations, that for the same peak voltage on the ring electrodes, the alternative running mode, PRSD, is more efficient than TWSD at high accelerations. This effect is caused by the larger Stark potential gradient for PRSD, which allows for larger accelerations before the stable phase-space region vanishes. The crossing point at which the two modes are equally efficient depends on the maximum applied voltage, among other experimental parameters. The PRSD mode is a particularly important option for use with lower applied voltages, and gives access to a previously inaccessible low-velocity regime. Thus PRSD provides a useful and straightforward method for decelerating many molecular species in a ring-geometry decelerator. These results could allow for more groups to be able to implement ring-geometry Stark deceleration using less challenging electronics, and still gain many benefits from the cylindrical symmetry of the electrodes.

Acknowledgments

We thank N Fitch for designing and constructing the decelerator system and high-voltage amplifiers, and D Macaluso for constructing the decelerator. This work was funded by NSF Grant No. CHE-1464997 and PHY-1734006 and AFOSR FA9550-16-0117.

ORCID iDs

Yomay Shyur https://orcid.org/0000-0001-5231-2397

References

[1] van Veldhoven J, Küpper J, Bethlem H L, Sartakov B, van Roij A J A and Meijer G 2004 *Eur. Phys. J.* D **31** 337–49
[2] Kirste M, Wang X, Schewe H C, Meijer G, Liu K, van der Avoird A, Janssen L M C, Gubbels K B, Groenenboom G C and van de Meerakker S Y T 2012 *Science* **338** 1060–3
[3] van de Meerakker S Y T, Vanhaecke N, van der Loo M P J, Groenenboom G C and Meijer G 2005 *Phys. Rev. Lett.* **95** 013003
[4] Gilijamse J J, Hoekstra S, Meek S A, Metsälä M, van de Meerakker S Y T, Meijer G and Groenenboom G C 2007 *J. Chem. Phys.* **127** 221102
[5] Hudson E R, Lewandowski H J, Sawyer B C and Ye J 2006 *Phys. Rev. Lett.* **96** 143004
[6] Bethlem H L, Kajita M, Sartakov B, Meijer G and Ubachs W 2008 *Eur. Phys. J. Spec. Top.* **163** 55–69
[7] Tarbutt M R, Hudson J J, Sauer B E and Hinds E A 2009 *Faraday Discuss.* **142** 37–56
[8] Bethlem H L, Berden G, Crompvoets F M H, Jongma R T, van Roij A J A and Meijer G 2000 *Nature* **406** 491–4
[9] van Veldhoven J, Bethlem H L, Schnell M and Meijer G 2006 *Phys. Rev.* A **73** 063408
[10] Gilijamse J J, Hoekstra S, Vanhaecke N, van de Meerakker S and Meijer G 2010 *Eur. Phys. J.* D **57** 33–41
[11] Sawyer B C, Lev B L, Hudson E R, Stuhl B K, Lara M, Bohn J L and Ye J 2007 *Phys. Rev. Lett.* **98** 253002
[12] Riedel J, Hoekstra S, Jäger W, Gilijamse J J, van de Meerakker S Y T and Meijer G 2011 *Eur. Phys. J.* D **65** 161–6
[13] van Veldhoven J, Bethlem H L and Meijer G 2005 *Phys. Rev. Lett.* **94** 083001
[14] Bethlem H L, Tarbutt M R, Küpper J, Carty D, Wohlfart K, Hinds E A and Meijer G 2006 *J. Phys. B: At. Mol. Opt. Phys.* **39** R263
[15] Schnell M, Lützow P, van Veldhoven J, Bethlem H L, Küpper J, Friedrich B, Schleier-Smith M, Haak H and Meijer G 2007 *J Phys. Chem.* A **111** 7411–9
[16] Gilijamse J J, Hoekstra S, van de Meerakker S Y T, Groenenboom G C and Meijer G 2006 *Science* **313** 1617–20
[17] van de Meerakker S Y T and Meijer G 2009 *Faraday Discuss.* **142** 113–26
[18] Scharfenberg L, van de Meerakker S Y T and Meijer G 2011 *Phys. Chem. Chem. Phys.* **13** 8448–56
[19] Scharfenberg L, Gubbels K B, Kirste M, Groenenboom G C, van der Avoird A, Meijer G and van de Meerakker S Y T 2011 *Eur. Phys. J.* D **65** 189–98
[20] Sawyer B C, Stuhl B K, Wang D, Yeo M and Ye J 2008 *Phys. Rev. Lett.* **101** 203203
[21] Sawyer B C, Stuhl B K, Yeo M, Tscherbul T V, Hummon M T, Xia Y, Klos J, Patterson D, Doyle J M and Ye J 2011 *Phys. Chem. Chem. Phys.* **13** 19059–66
[22] Parazzoli L P, Fitch N J, Żuchowski P S, Hutson J M and Lewandowski H J 2011 *Phys. Rev. Lett.* **106** 193201
[23] Bethlem H L, Berden G and Meijer G 1999 *Phys. Rev. Lett.* **83** 1558–61
[24] van de Meerakker S Y T, Vanhaecke N, Bethlem H L and Meijer G 2006 *Phys. Rev.* A **73** 023401
[25] Scharfenberg L, Haak H, Meijer G and van de Meerakker S Y T 2009 *Phys. Rev.* A **79** 023410
[26] Parazzoli L P, Fitch N, Lobser D S and Lewandowski H J 2009 *New J. Phys.* **11** 055031
[27] Hou S, Li S, Deng L and Yin J 2013 *J. Phys.* B **46** 045301
[28] Meek S A, Bethlem H L, Conrad H and Meijer G 2008 *Phys. Rev. Lett.* **100** 153003
[29] Meek S A, Conrad H and Meijer G 2009 *New J. Phys.* **11** 055024
[30] Meek S A, Conrad H and Meijer G 2009 *Science* **324** 1699–702
[31] Osterwalder A, Meek S A, Hammer G, Haak H and Meijer G 2010 *Phys. Rev.* A **81** 051401
[32] Meek S A, Parsons M F, Heyne G, Platschkowski V, Haak H, Meijer G and Osterwalder A 2011 *Rev. Sci. Instrum.* **82** 093108

[33] van den Berg J, Mathavan S, Meinema C, Nauta J, Nijbroek T, Jungmann K, Bethlem H and Hoekstra S 2014 *J. Mol. Spectrosc.* **300** 22–5
[34] van den Berg J E, Turkesteen S H, Prinsen E B and Hoekstra S 2012 *Eur. Phys. J.* D **66** 235
[35] Bulleid N E, Hendricks R J, Hinds E A, Meek S A, Meijer G, Osterwalder A and Tarbutt M R 2012 *Phys. Rev.* A **86** 021404
[36] Mathavan S C, Zapara A, Esajas Q and Hoekstra S 2016 *Chem. Phys. Chem.* **17** 3709–13
[37] Quintero-Pérez M, Jansen P, Wall T E, van den Berg J E, Hoekstra S and Bethlem H L 2013 *Phys. Rev. Lett.* **110** 133003
[38] Jansen P, Quintero-Pérez M, Wall T E, van den Berg J E, Hoekstra S and Bethlem H L 2013 *Phys. Rev.* A **88** 043424
[39] Quintero-Pérez M, Wall T E, Hoekstra S and Bethlem H L 2014 *J Mol. Spectrosc.* **300** 112–5
[40] Meng C, van der Poel A P P, Cheng C and Bethlem H L 2015 *Phys. Rev.* A **92** 023404
[41] Hou S, Wang Q, Deng L and Yin J 2016 *J. Phys.* B **49** 065301
[42] Ashfold M, Langford S, Morgan R, Orr-Ewing A, Western C, Scheper C and de Lange C 1998 *Eur. Phys. J* D **4** 189–97
[43] Bethlem H L, Crompvoets F M H, Jongma R T, van de Meerakker S Y T and Meijer G 2002 *Phys. Rev.* A **65** 053416
[44] Friedrich B 2004 *Eur. Phys. J.* D **31** 313–36